Numerical Simulation of Contraction Flows of Newtonian Fluid Using Taylor Galerkin Pressure Correction Finite Element Method

Alaa A Sharhan[1,*], Alaa H. Al-Muslimawi[1], Ihssan A. Fadhel[2]

1. Department of Mathematics, College of Science, University of Basrah, Basra, IRAQ
2. Ministry of Education \ General Directorate of Education of Basra, IRAQ
*Corresponding author E-mail: eala.khashab.sci@uobasrah.edu.iq

Doi:10.29072/basjs.20230202

ARTICLE INFO

Keywords

Contraction flow; Newtonian fluid; Taylor Galerkin finite element method; Navier-Stokes equation.

ABSTRACT

In this study, numerical simulation of Newtonian fluids in contraction channels is performed based on the Taylor Galerkin-pressure correction finite element method (TGPC-FEM). Here, three different contraction channel geometries (4:1, 6:1, and 8:1) were simulated in this investigation. Usually, the continuity equation and momentum equation are governed this type of fluid. These equations are presented in our study in cylindrical coordinate system. This research examined the impact of varying Reynolds number and geometry area difference on the rate of convergence for solution components, as well as the influence of geometry area difference on level of velocity and pressure.

Received 26 Dec 2022; Received in revised form 28 Feb 2023; Accepted 13 May 2023, Published 31 Aug 2023

1. Introduction

The study of fluid flow through contraction channels is critical for a variety of reasons, including its importance to human health and technological advancement. Fluid dynamics in abrupt contraction channels have been extensively studied, and many of these works have been published in the last few years (see, for example, [1–5]). In addition, in the fluid dynamics, we need a governing equations to describe the behavior of fluid. In this area the Navier-Stokes equations represent one of the most important model that is used to address the fluid flow. These equations consist of mass conservation equation (continuity equation) and momentum conservation [6, 7]. The main difficulty that faced by scientists when studying this type of equations is the inability to find out the exact solutions, which required resorting to numerical methods to overcome this problem. A Taylor-Galerkin pressure-corrected finite element technique is a very good option for resolving this issue with the Navier-Stokes equation. Townsend and Webster [8] were the first to suggest this strategy as a method for dealing with incompressible flows, including Newtonian and non-Newtonian fluids. This approach involves two methods, a Taylor Galerkin method and a pressure correction method. The Taylor Galerkin method is a two-step Lax-Wendroff time stepping procedure (predictor-corrector), extracted via a Taylor series expansion in time (Donea [9]). The pressure-correction method accommodates the incompressibility constraint to ensure second-order accuracy in time. The numerical solution of these equations involves the use of efficient and precise numerical techniques and methodologies. Many researchers have presented studies and research on a numerical solution using this method (see [10-14]). Thus, literature on (TGPC-FEM) for fluid flows is covered broadly (see for example [15-18]). The novelty of this work is studying Newtonian fluid flow in 4:1, 6:1, and 8:1 abrupt contraction channel using the Taylor Galerkin pressure correction finite element approach. This study focuses on fluid flow behavior under the influence of different Reynolds numbers and flow channel geometries. This research also discusses the behavior of velocity and pressure along the axis of symmetry under the impact of geometric change. The mathematical model was the subject of the second section of this research project. We detailed the problem definition and boundary conditions, as well as the numerical approach used to solve the governing equation in the mathematical model represented by the (TGPC-FEM) in the third and fourth sections. Showing and discussing the results was done in the fifth section of this research.

2. Mathematical modeling

The governing equations, which consist of continuity and momentum equations under isothermal condition and ignoring anybody forces may be present:

$$\nabla \cdot u = 0, \tag{1}$$

$$\rho\left(\frac{\partial u}{\partial t} + u \cdot \nabla u\right) = -\nabla p + \nabla \cdot (2\mu_s d). \tag{2}$$

The solvent viscosity (μ_s), density (ρ), hydrodynamic pressure (p), and velocity (u) are the four parameters in these equations. In addition to that, the deformation tensor, is represented by the equation $d = \frac{1}{2}(\nabla u + \nabla u^{\tau})$. By using the scaling $Re = \rho\frac{UL}{\mu}$, the equation (Navier-Stokes) may also be written in terms of non-dimensional (Re) groups, where (U), (L), and (ρ) stand for the usual flow velocity, length, and density, respectively. Thus, the Newtonian version of the momentum equation can be written in a non-dimensional form as follows:

$$Re\left(\frac{\partial u}{\partial t} + u \cdot \nabla u\right) = -\nabla p + \nabla \cdot (2\mu_s d). \tag{3}$$

3. Numerical method

Three phases make up (TGPC-FEM), which employs a fractional step approach. To begin, we use a two-steps predictor-corrector technique to calculate the u^* components, using the initial velocity and pressure fields as inputs. In the second stage, we use the Choleski method to determine the pressure difference $(P^{n+1} - P^n)$ and set u^* as the controlling variable. In the third stage, we utilize the pressure difference $(P^{n+1} - P^n)$ and mid velocity (u^*) to make an estimate for the velocity field (u^{n+1}). As a direct consequence of this, the fractional step may be written as follows:

$$\text{Stage1a:}\frac{2Re}{\Delta t}\left[u^{n+\frac{1}{2}} - u^n\right] = L(u^n, d^n) - \nabla p^n, \tag{4}$$

$$\text{Stage1b:}\frac{Re}{\Delta t}[u^* - u^n] = L\left(u^{n+\frac{1}{2}}, d^{n+\frac{1}{2}}\right) - \nabla p^n, \tag{5}$$

$$\text{Stage2:}\nabla^2(p^{n+1} - p^n) = \frac{Re}{\theta\Delta t}\nabla \cdot u^*, \tag{6}$$

$$\text{Stage3:}\, u^{n+1} = u^* - \frac{\theta\Delta t}{Re}[\nabla(p^{n+1} - p^n)]. \tag{7}$$

Where,

$$L(u,d) = [\nabla \cdot (2\mu_s d) - \mathrm{Re}\ u \cdot \nabla u]. \quad (8)$$

For θ=1/2 the methodology employed in the solution is based on the Crank-Nicolson method, which provides better accuracy and stability compared to other methods and decreases time errors in the time-stepping scheme [19,20]. The following formulas can be used to calculate velocity and pressure findings:

$$u(x,t) = \sum_{j=1}^{Ju} u_j(t)\phi_j(x), \quad (9)$$

$$p(x,t) = \sum_{j=1}^{Jp} p_j(t)\psi_j(x), \quad (10)$$

Specifically, J_u is the total number of nodes, and J_p is the number of nodes at triangular vertices only. The nodal values of the velocity and pressure vectors are denoted by u_j(t) and p_j(t), respectively. Fundamental interpolation functions for their respective numerical method are $\phi_j(x)$ and $\psi_j(x)$, respectively. u^* as well as pressure difference may both be represented using forms that are related to one another. Segmenting the domain Ω to trigonometric elements is very important to get very accurate results. When dealing with a triangular, both the mid-side and vertex nodes are utilized to compute velocity, but only the vertex nodes are used to compute pressure. The shape functions $\phi_j(x)$ have been selected for use as the quadratic basis function, and the shape function $\psi_j(x)$ have been selected for use as the linear basis function. Then, a matrix form of the TGPC corresponding to Equations (4-7), respectively, may be represented as follows [21].

$$\text{Step1a:}\left[\frac{2Re}{\Delta t}M + \frac{\mu_s}{2}S\right]\left(U^{n+\frac{1}{2}} - U^n\right) = \{-[\mu_s S + Re\ N(U)]U + \ell^T P\}^n, \quad (11)$$

$$\text{Step 1b: } \left[\frac{Re}{\Delta t}M + \frac{\mu_s}{2}S\right](U^* - U^n) = \{-\mu_s SU + \ell^T P\}^n - Re\,[N(U)U]^{n+\frac{1}{2}}, \quad (12)$$

$$\text{Step2: } K(P^{n+1} - P^n) = -\frac{Re}{\theta\Delta t}\ell U^*, \quad (13)$$

$$\text{Step3: } \frac{Re}{\Delta t}M(U^{n+1} - U^*) = \theta\ell^T(P^{n+1} - P^n). \quad (14)$$

In this context, U^n, U^{n+1} and P^n, P^{n+1} are the velocity and pressure nodal vectors at time t^n and t^{n+1}, respectively. U^* is an intermediate nodal velocity vector established in Step 1b. According to [22], *M, S, N, ℓ*, and *K* stand in for the matrices for mass, momentum diffusion, convection, divergence/pressure gradient, and pressure stiffness, respectively.

Where

$$M_{ij} = \int_{\Omega} \phi_i \phi_j d\Omega, \quad K_{ij} = \int_{\Omega} \nabla\psi_i \nabla\psi_j d\Omega, \quad N(U)_{ij} = \int_{\Omega} \phi_i (U^n . \nabla\phi_j) d\Omega$$

$$(\ell)_{ij} = \int_{\Omega} \psi_i (\nabla . \phi_j)\, d\Omega, \quad (S)_{ij} = \int_{\Omega} \left[\nabla\phi_j : \nabla\phi_j + (\nabla\phi_j)^{\tau}\right] d\Omega.$$

4. Problem specification and boundary conditions

The benchmark problem for this study is the flow of Newtonian fluid under isothermal condition via a contraction channel with a two-dimensional axisymmetric shape and contraction with ratios of 4:1 sharp, 6:1 sharp, and 8:1 sharp. Thus, the breadth of the outlet of all channels is only one unit long, while the length of the broad section of all channels is equal to ten units and the length of the narrow part of all channels is equal to four units. Whereas the width of the input for all channels is, correspondingly, 4, 6, and 8 units of length. In addition, the trigonometric elements of the meshes of the geometric figures of the constriction channels were taken in the same size region so that the study on the influence of changing the geometric figure on the constriction channel could be more accurate and objective. All of the different forms of mesh have been included, and the corresponding schematics for the various geometric configurations can be seen in detail in Figure 1. The characteristics of the finite element meshes used in our research are outlined in Table 1.

Boundary conditions (*BCs*): The following describes the present configuration of the BC:

(a) At the inlet of the channel, there is no radial velocity, and the flow is alluded to as Poiseuille (*Ps*) flow which denoted by $u_z = 2(1 - \frac{r^2}{R^2})$, where R denotes the channel's radial and $0 \leq r \leq R$. The values of channels radial (R) with contraction ratios of 4:1, 6:1 and 8:1 are 4, 6 and 8 respectively.

(b) There is neither axial velocity nor radial velocity along the bottom wall of the channel.

(c) The axial velocity is slipping on the axially symmetric line of the channel, whereas the radial velocity has no slip.

(d) At the channel's outlet, there is no pressure.

All details for above are presented in Figure 2.

Table 1: statically of meshes elements

Mesh	Total Elements	Total Nodes	Boundary Nodes	Pressure Nodes
4:1 sharp contraction	1128	2387	244	639
6:1 sharp contraction	1640	3419	276	890
8:1 sharp contraction	2152	4460	308	1154

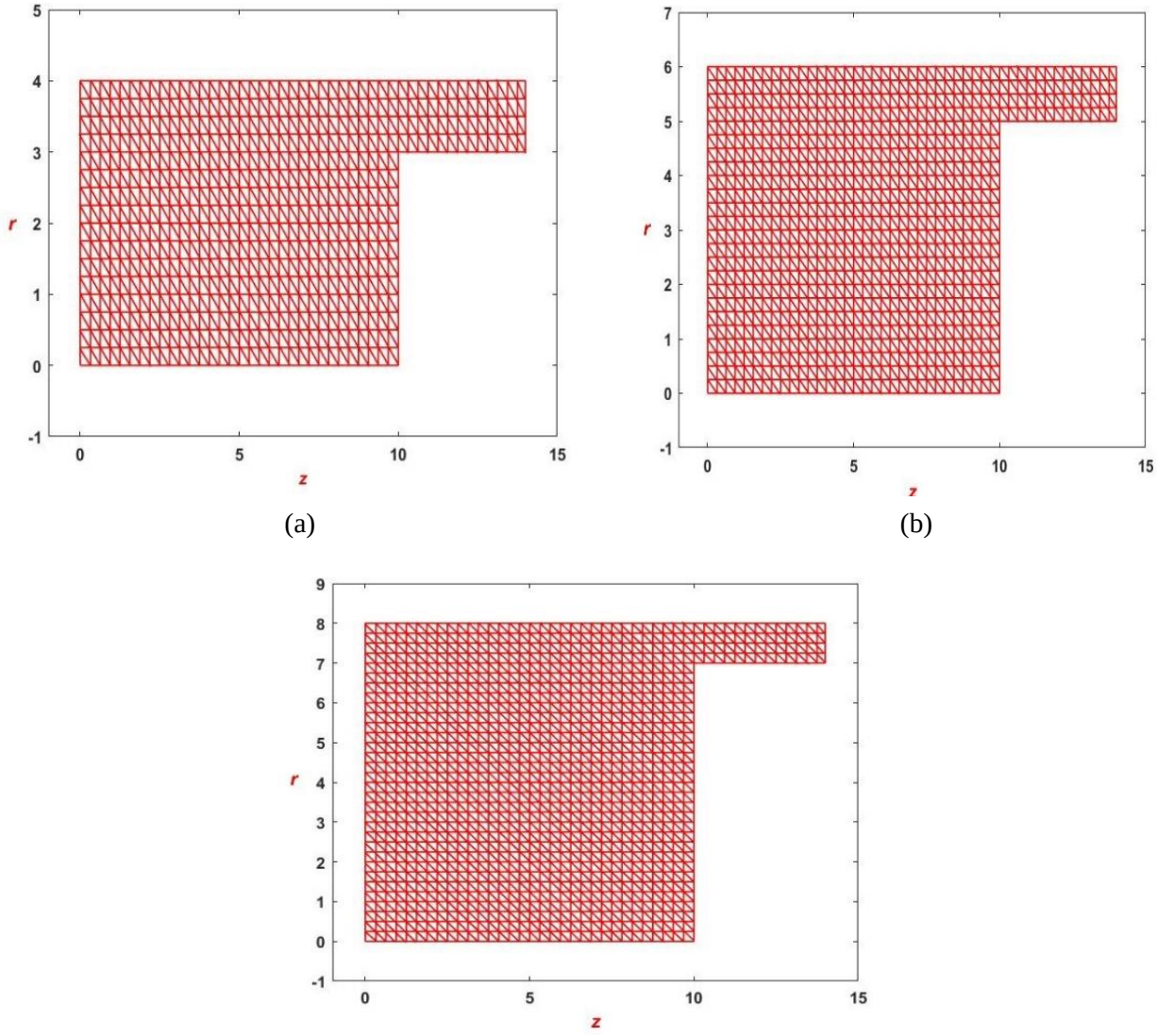

Figure 1: Structured finite element meshes (a) 4:1 sharp contraction (b) 6:1 sharp contraction (c) 8:1 sharp contraction

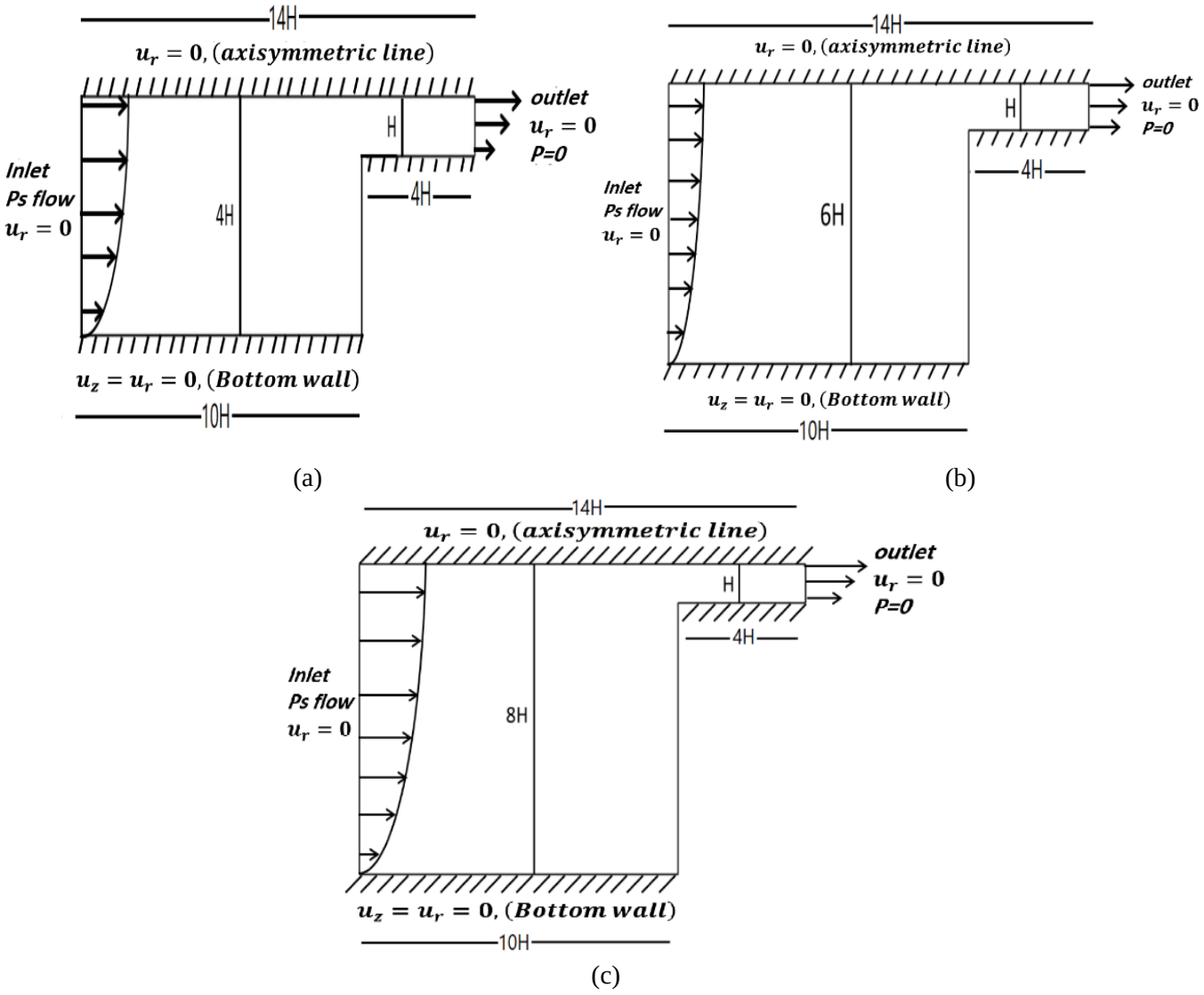

Figure 1: Flow geometry (a) 4:1 sharp contraction (b) 6:1 sharp contraction (c) 8:1 sharp contraction

5. Numerical results

The flow fields of velocity and pressure are shown in Figure 3 for 4:1, 6:1 and 8:1 contraction channel with constant fluid parameters (*Re*=1 and μ_s =1). In all cases, according to the scales of the velocity field, that the velocity rises as we go closer to the outflow of the channel, and reaching to the maximum value at the outlet. That is, the velocity increases in the narrow section of the channel, and this is a clear application of the continuity equation ($A_1u_1 = A_2u_2$), where the

velocity increases when the area decreases [23]. This is a straightforward illustration of Bernoulli's principle, where the pressure exhibits the opposite behavior, that is, the pressure reduces as we go closer to the outlet of the channel in contrast to the velocity, which increases. In addition, we can see that the value of velocity that is present at the outlet of the contraction channel 8:1 is greater than the value of velocity that is present at the outlet of the contraction channel 6:1 and 4:1, despite the fact that all of these channels have the same diameter of the outlet. This is according to the continuity equation, a higher velocity at the outlet is required for the 8:1 channel since its wide section has a bigger area than the 6:1 and 4:1 channel's wide section. Table 2 shows data for the maximum velocity and pressure values in the three contraction channels and various Reynolds numbers. The results showed that increasing Reynolds number causes a decrease in the maximum fluid velocity, indicating that the relationship is inverse. From physical perspective, a rise in the density, as related by the Reynolds number, results in a decrease in velocity. As the embodiment of Bernoulli's principle, pressure behavior is the opposite of velocity behavior with respect to the relationship with Reynolds number. Moreover, the rise in density that relate with the Reynolds number results in an increase in the obstruction to fluid flow, which results in higher pressure.

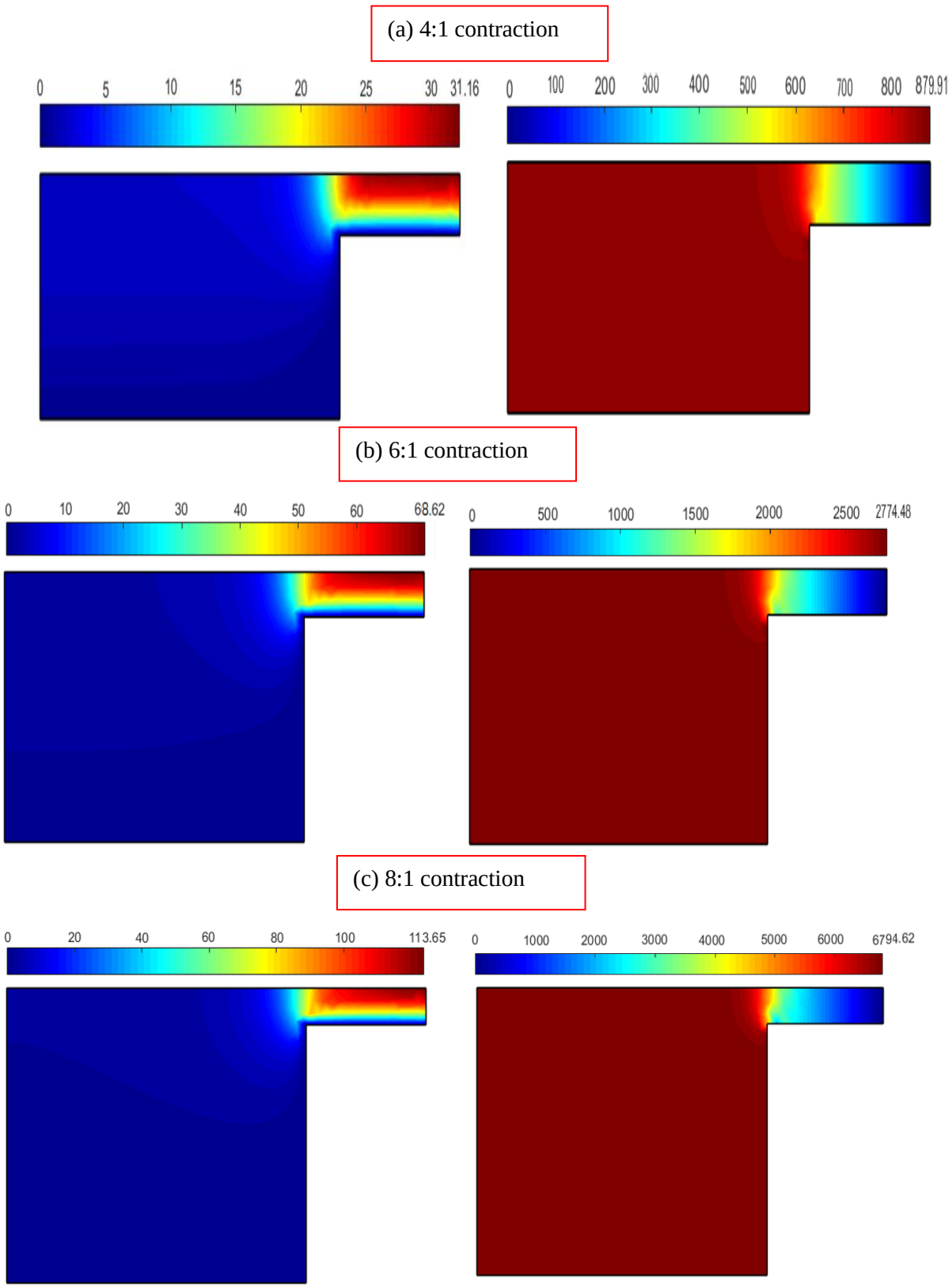

Figure 3: Velocity and pressure fields of; (a) 4:1 contraction (b) 6:1 contraction, (c) 8:1 contraction

Table 2: Max velocity and pressure for contraction channels with variation *Re*

Re	4:1 contraction		6:1 contraction		8:1 contraction	
	Max v	Max p	Max v	Max p	Max v	Max p
1	31.16	879.91	68.62	2774.48	113.65	6794.62
2	30.9	1162.4	62.95	4105.89	105.73	10639.47
3	29.55	1434.4	59.03	5334.87	103.72	14220.02
4	28.29	1692.69	56.6	6505.49	101.5	17668.48
5	27.24	1940.54	56.14	7645.83	100.66	20881.22
6	26.37	2180.12	55.49	8769.6	99.89	23364.18

The velocity and pressure trajectories along the axis of symmetry are shown in (a) and (b), respectively, in Figure 4 for a constant set of parameters {Re = 5 and μ_s = 1} and a variety of geometries. The relationship between the velocity and the length of the axis of symmetry is a direct relationship, that is, the velocity increases with the increase in the distance crossed from z, and it is the maximum possible in the outlet. The influence of geometry area variation on increasing the velocity along the axis of symmetry is considerable. Refer to Figure 3 for more information on the behavior of the velocity and pressure.

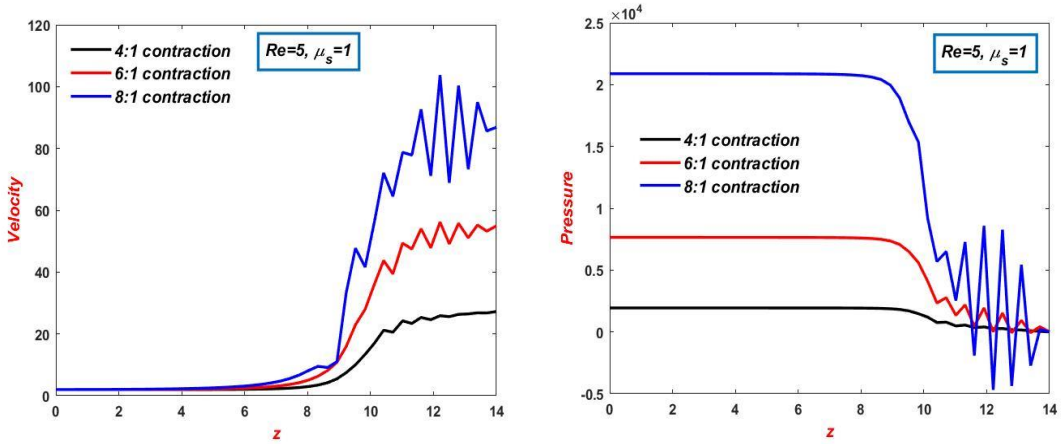

(a) (b)

Figure 4: Axisymmetric line profile with μ_s =1, *Re*=5, geometry variation; (a) velocity, (b) pressure

The convergence rate of velocity and pressure is shown in Figure 5 with constant parameters (*Re* = 5 and μ_s = 1) for three setting of contraction. According to the findings, a higher convergence rate was shown by expanding the geometry surface area, in both velocity and pressure convergence rates. The reason for this is obvious: as we have demonstrated before, increasing the number of elements used to split geometry increases the amount of time needed to solve.

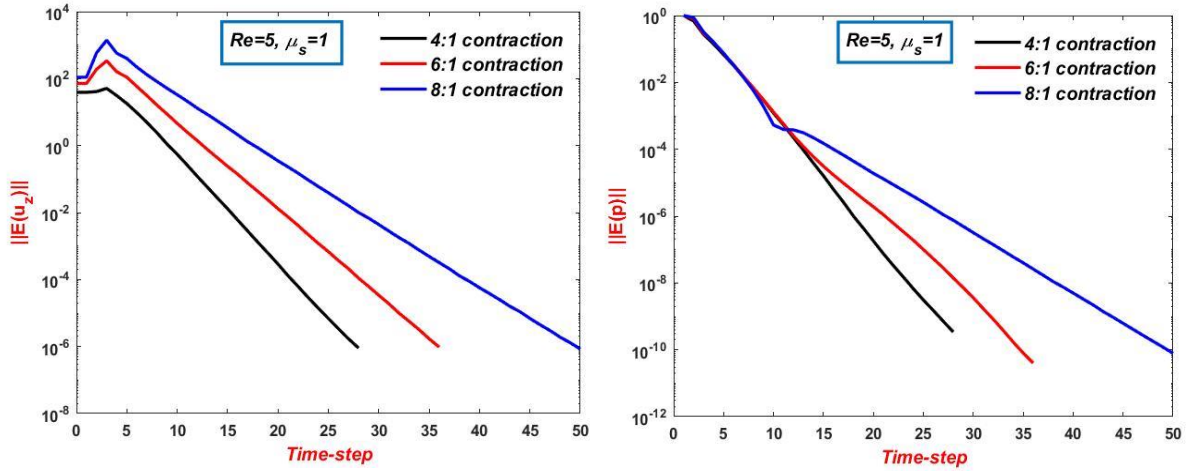

(a) (b)

Figure 5: Convergence profile with μ_s =1, *Re*=5, geometry variation; (a) velocity, (b)pressure

The Reynolds number has a considerable influence on the rate of convergence of velocity and pressure. When the Reynolds number approaches its critical value, the convergence rates increase substantially, and vice versa. Table 3 illustrates the critical level of Reynolds number values for each contraction channel. The results demonstrated that when the contraction ratio of the flow channel increases, the critical level of Reynolds number decreases. Therefore, we notice that in this work, the critical Reynolds number is as high as possible in the 4:1 contraction channel and as low as possible in the 6:1 contraction channel. As previously demonstrated in Figure 5, the rate of contraction is directly correlated with the velocity, and the velocity is inversely proportional to the Reynolds number, as indicated in Table 2. So, we conclude that there is an inverse relationship between the Reynolds number and the flow channel's contraction ratio.

Table 3: Critical Reynolds number for contraction channels

Contraction channel	Critical Reynolds number (Re_{cri})
4:1	30
6:1	11
8:1	6

Convergence of velocity in a 4:1, 6:1 and 8:1 contraction channels under varying Reynolds number (*Re*) is shown in Figure 6. The convergence rates of velocity were shown to rise noticeably with rising Reynolds numbers. It may be said that there is a direct relationship between *Re* and the rate of velocity convergence. Increasing the Reynolds number causes it to approach its critical value, which necessitates more time steps to reach the solution and is terminated when the error reaches (E= 10^{-6}). The geometry 8:1 has a greater rate of convergence than that in the case of 6:1 and 4:1. This is due to the fact that an increase in the geometry size results in an increase in the number of elements on which the geometry has been split. So, when the number of elements increases, the number of equations also goes up, which means you need more time to get the steady state solution. Moreover, under the same setting of parameters the pressure convergence has same behaviors of velocity (see Figure 7). Through the current study, the normal stress τ_{zz} and first normal stress N_1=$\tau_{zz} - \tau_{rr}$ along the centerline are illustrated in Figure. 8, for different setting of *Re* = 1, 2, 3, 4, 5. For both components, a constant τ_{zz} and N_1 levels are occurred through the channel section, with increase and then sharp decrease over that contraction region, with decline at the outlet. From the profiles one can observe that the maximum level of τ_{zz} and N_1 increases when *Re* is raised with high level in N_1. For example, with *Re*=10 the maximum level of N_1 is around 85 units, compared to 54 units with *Re*=1; almost *O*(36%) reduction.

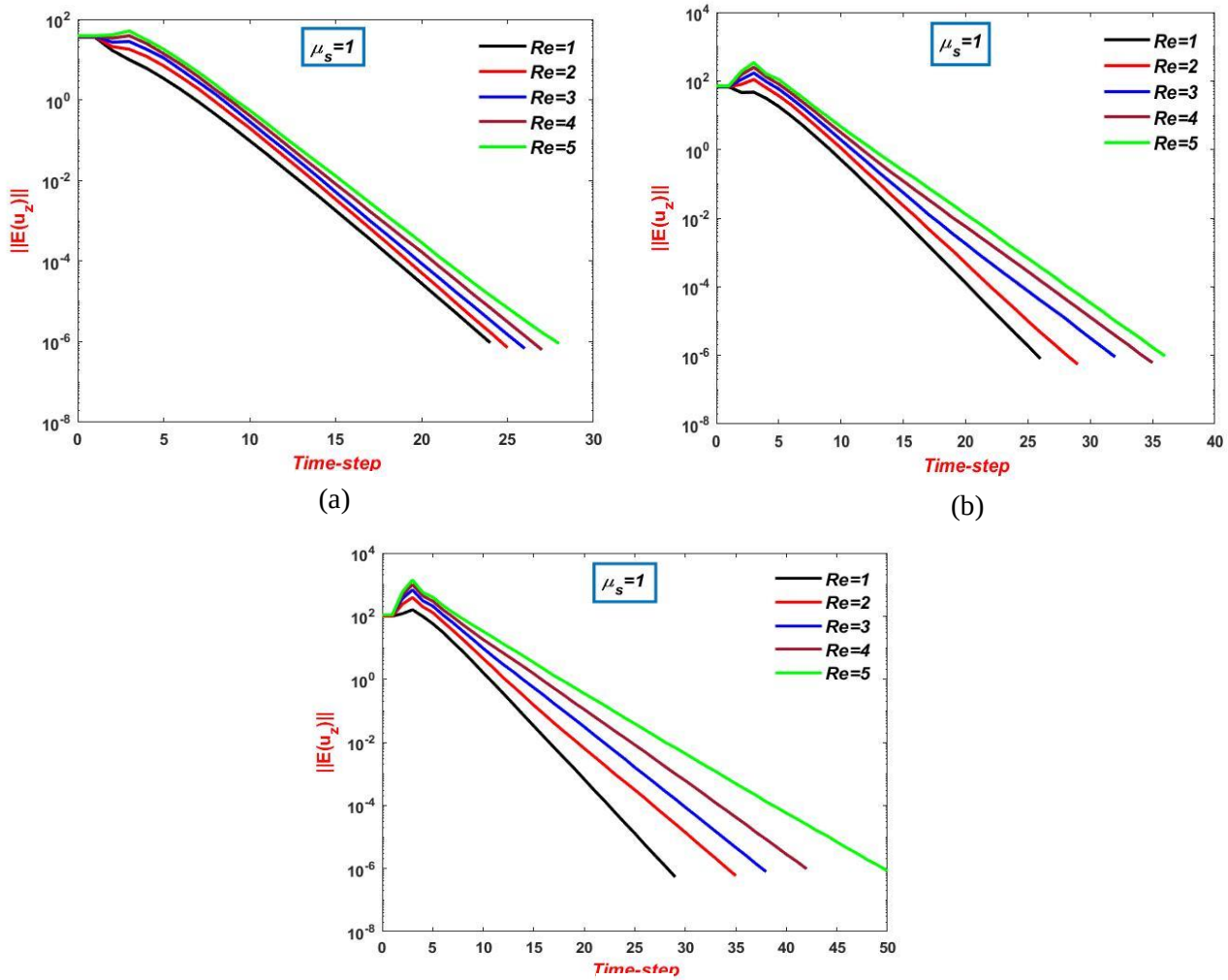

Figure 6: Convergence of velocity with with μ_s =1, *Re* variation; (a) 4:1 contraction, (b) 6:1 contraction, (c) 8:1 contraction

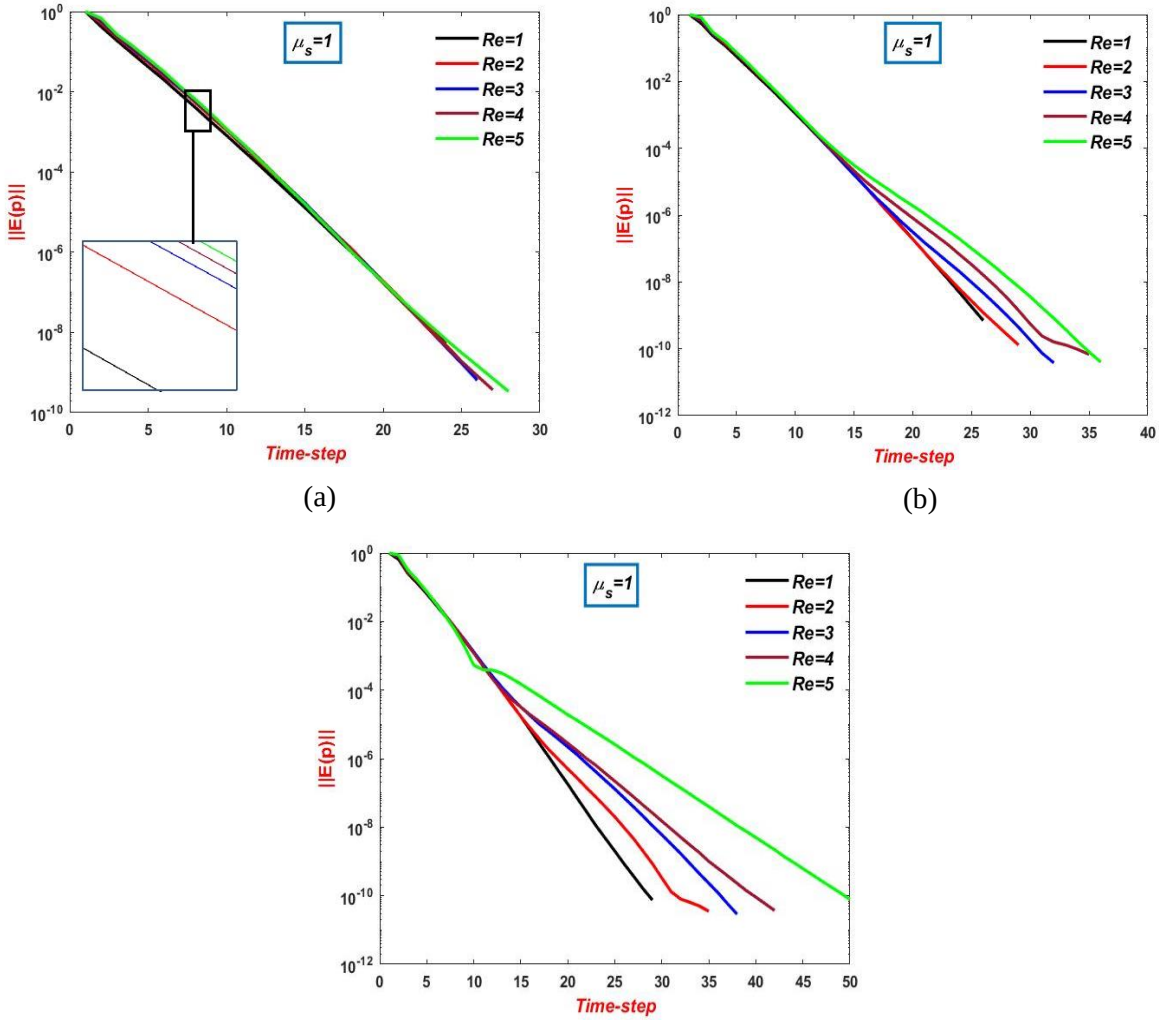

Figure 7: Convergence of pressure with $\mu_s = 1$, Re variation; (a) 4:1 contraction, (b) 6:1 contraction, (c) 8:1 contraction

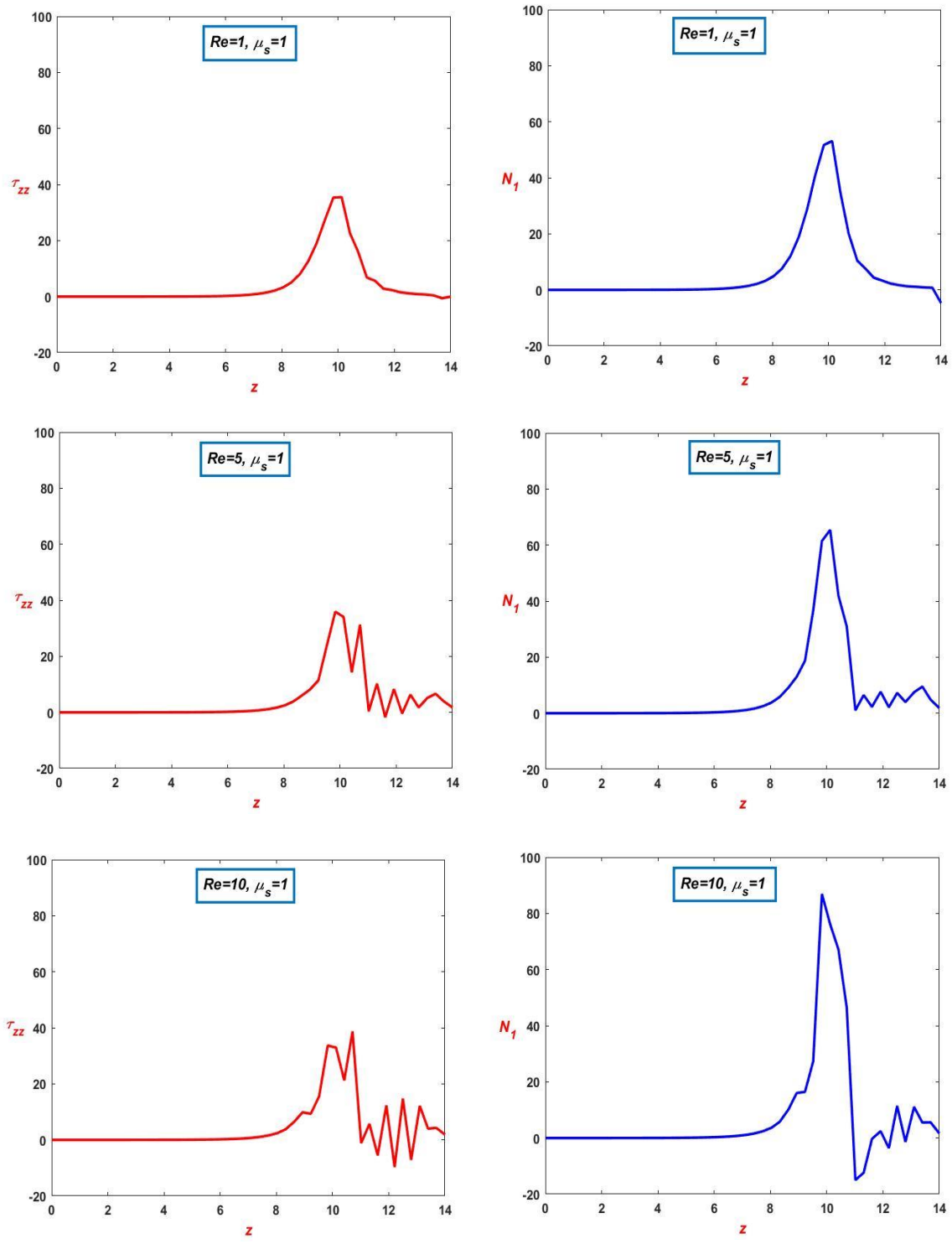

Figure 8: Normal stress (τ_{zz}), first normal stress (N_1) with μ_s =1, *Re* variation; 4:1 contraction

6. Conclusions

Using the Taylor-Galerkin pressure correction finite element method, this study investigates the effects of varying the Reynolds number and the contraction geometry on the behavior of fluid flow. From the results, one can see that the maximum velocity decreases as the Reynolds number rises, whereas the maximum pressure increases. An increase in the Reynolds number will produce an increase in the rate of convergence for both the velocity and the pressure. The rates of convergence for velocity and pressure go up as the size of geometry contraction increases. Therefore, the 8:1 flow channel has a larger level of convergence compared to 6:1 and 4:1 flow. Furthermore, as the flow channel's geometry area is increased, the velocity and pressure along the axis of symmetry of the flow channel also rise. An inverse correlation exists between the contraction ratio of the flow channel and the critical Reynolds number.

References

[1] D. M. Binding, Further considerations of axisymmetric contraction flows, J. Non-Newt. Fluid Mech., 41(1991) 27-42. https://doi.org/10.1016/0377-0257(91)87034-U

[2] O. J. David, G. G. Fuller, Contraction and expansion flows of Langmuir monolayers, J. Non-Newt. Fluid Mech., 89(2000)187-207, https://doi.org/10.1016/S0377-0257(99)00024-5

[3] S. Nigen, K. Walters, Viscoelastic contraction flows: comparison of axisymmetric and planar configurations, J Non-Newt. Fluid Mech., 102(2002)343-359, https://doi.org/10.1016/S0377-0257(01)00186-0

[4] M. Blanco, J. Battiato, J. K. Disotell, Sensitivity Study of Contraction Flow for Boundary-Layer Validation Wind Tunnel, AIAA Aviation 2019 Forum. 2019, https://doi.org/10.2514/6.2019-3095

[5] J. H. Simon et al, Flow of dilute to semi-dilute polystyrene solutions through a benchmark 8: 1 planar abrupt micro-contraction, J. Non-Newt. Fluid Mech., 165(2010) 1654-1669. https://doi.org/10.1016/j.jnnfm.2010.09.002

[6] Z.U. Warsi, Conservation form of the Navier-Stokes equations in general nonsteady coordinates, AIAA J,19(1981)240-242, https://doi.org/10.2514/3.7763

[7] S. Farzin, T.J.R Hughes, Zdeněk Johan, A new finite element formulation for computational fluid dynamics: X. The compressible Euler and Navier-Stokes equations, Comp. Meth. App Mech. Eng., 89(1991)141-219, https://doi.org/10.1016/0045-7825(91)90041-4

[8] V. Ngamaramvaranggul, M.F. Webster, Computation of Free Surface Flows with a Taylor-Galerkin/Pressure-correction Algorithm, Int. J. Num. Meth. Fluids, 27(1999), https://doi.org/10.1016/j.cam.2016.06.007

[9] J. Donea, A Taylor–Galerkin method for convective transport problems, Int. J. Num. Meth. Eng., (1984) 101–119. https://doi.org/10.1002/nme.1620200108

[10] A. H. Al-Muslimawi, Taylor Galerkin pressure correction (TGPC) finite element method for incompressible Newtonian cable-coating flows, J. Kufa Math. Comp., 5(2018)14-22, https://doi.org/10.31642/JoKMC/2018/050203

[11] A. Sharhan, A. H. Al-Muslimawi, Numerical Study of Shear and Extensional Inelastic Contraction Flows,. *CFD Letter,s* 15(2023)107-121, https://doi.org/10.37934/cfdl.15.8.107121

[12] A. Fadhel, A. H. Al-Muslimawi, Simulation of Newtonian axisymmetric pipe flow by using a Taylor Galerkin/pressure correction finite element method, *Bas. J. Sci* 38(2020)198-222, doi 10.29072/basjs.202024

[13 A. Sharhan, A. Al-Muslimawi, Numerical simulation of a power-law inelastic fluid in axisymmetric contraction by using a Taylor Galerkin-pressure correction finite element method, Int. J. Non-line. Anal. App. 12, Special Issue (2021)2211-2222, http://dx.doi.org/10.22075/ijnaa.2021.6113

[14] V. Ngamaramvaranggul, M.F. Webster, Viscoelastic simulations of stick-slip and die-swell flows, Int. J. Num. Meth. Fluids 36(2001)539-595, https://doi.org/10.1002/fld.145

[15] A. Baloch, P. Townsend, M.F. Webster, On two-and three-dimensional expansion flows, Comp. Fluids, 24(1995)863-882, https://doi.org/10.1016/0045-7930(95)00020-D

[16] P. Rameshwaran, P. Townsend, M. F. Webster, Simulation of Particle Setting in Rotating and Non-Rotating Flow of Non-Newtonian Fluids, Int. J. Num. Meth. Fluids, 26(1998) 851-874 , https://doi.org/10.1002/(SICI)1097-0363(19980415)26

[17] A.H. Al-Muslimawi, Theoretical and numerical studies of die swell flow, Korea-Australia Rheology J, 28(2016)229-236, https://doi.org/10.1007/s13367-016-0023-6

[18] A. H. Al-Muslimawi, H.R. Tamaddon-Jahromi, M.F. Webster, Simulation of viscoelastic and viscoelastoplastic die-swell flows, J. Non-Newt. Fluid Mech., 191 (2013) 45-56, https://doi.org/10.1016/j.jnnfm.2012.08.004

[19] B. Jin, B. Li, Z. Zhou, An analysis of the Crank-Nicolson method for subdiffusion, IMA J. Num. Anal., 38(2018)518-541, https://doi.org/10.48550/arXiv.1607.06948

[20] M Mu, Y. Huang, An alternating Crank--Nicolson method for decoupling the Ginzburg--Landau equations. SIAM J. Num. Anal., 35(1998)1740-1761, https://doi.org/10.1137/S0036142996303092

[21] M. Aboubacar, H. Matallah, and M. F. Webster, Highly elastic solutions for Oldroyd-B and Phan-Thien/Tanner fluids with a finite volume/element method: planar contraction flows J. Non-Newt. Fluid Mech., 103(2002)65-103, https://doi.org/10.1016/S0377-0257(01)00164-1

[22] A. J. Davies, The finite element method: An introduction with partial differential equations, OUP Oxford (2011).

[23] B. Şahin, A.J. Ward-Smith, D. Lane, The pressure drop and flow characteristics of wide-angle screened diffusers of large area ratio, J. Wind Eng. Industrial Aerodynamics 58(1995)33-50, https://doi.org/10.1016/0167-6105(95)00018-M

محاكاة عددية لتدفقات الانكماش للموائع النيوتونية باستخدام طريقة تايلور جاليركين لتصحيح الضغط للعناصر المحددة

علاء عبدالواحد شرهان[1], علاء حسن عبدالله[2], احسان فاضل عقيل[3]

[1]قسم الرياضيات /كلية العلوم /جامعة البصرة, البصرة /العراق

[2]قسم الرياضيات /كلية العلوم /جامعة البصرة, البصرة /العراق

[3]المديرية العامة لتربية البصرة, البصرة/ العراق

المستخلص

في هذه الدراسة، تم إجراء محاكاة عددية للموائع النيوتونية في قنوات الانكماش باستخدام طريقة تايلر جاليركين لتصحيح الضغط للعناصر المحددة (.(TGPC-FEM هنا، تم محاكاة ثلاثة أشكال هندسية مختلفة لقناة الانكماش (4:1، 6:1، و8:1) في هذا البحث. معادلة الاستمرارية ومعادلة الزخم هما المعادلتان الحاكمتان هذا النوع من الموائع. تم تقديم هذه المعادلات في دراستنا في نظام الإحداثيات الأسطوانية. وقد تناول هذا البحث تأثير اختلاف عدد رينولدز وفرق المساحة الهندسية على معدل التقارب لمكونات المحلول، وكذلك تأثير اختلاف المساحة الهندسية على مستوى السرعة والضغط.